Bioactive Materials 35 (2024) 564–576

Contents lists available at ScienceDirect

Bioactive Materials

journal homepage: www.keaipublishing.com/en/journals/bioactive-materials

Apoptotic extracellular vesicles restore homeostasis of the articular microenvironment for the treatment of rheumatoid arthritis

Xian Li [a,c], Shichun Li [b], Xiaoling Fu [b,d,*], Yingjun Wang [c,e,**]

[a] School of Materials Science and Engineering, South China University of Technology, Guangzhou, 510641, China
[b] School of Biomedical Sciences and Engineering, South China University of Technology, Guangzhou International Campus, Guangzhou, 511442, China
[c] National Engineering Research Center for Tissue Restoration and Reconstruction and Innovation Center for Tissue Restoration and Reconstruction, Guangzhou, 510006, China
[d] Key Laboratory of Biomedical Engineering of Guangdong Province, South China University of Technology, Guangzhou, 510006, China
[e] NMPA Key Laboratory for Research and Evaluation of Innovative Biomaterials for Medical Devices, Guangzhou, 510700, China

ARTICLE INFO

Keywords:
Apoptotic extracellular vesicles
Microenvironment homeostasis
Rheumatoid arthritis

ABSTRACT

Rheumatoid arthritis (RA) is a severe autoimmune disease with symptoms including synovial inflammation, cartilage erosion, and bone loss in RA lesions, which eventually lead to joint deformity and function loss. Most current treatments fail to achieve satisfying therapeutic outcomes with some adverse effects. Extracellular vesicles derived from apoptotic cells (apoEVs) have emerged as important mediators in intercellular communication regulating diverse physiological and pathological processes. In this study, we investigated the therapeutic efficacy of macrophage-derived and osteoclast-derived apoEVs (Mφ-apoEVs and OC-apoEVs) on RA. The *in vitro* results showed that both Mφ-apoEVs and OC-apoEVs induced macrophage repolarization toward the anti-inflammatory M2 phenotype, promoted chondrocyte functions and chondrogenesis, and inhibited osteoclast formation and maturation. In addition, OC-apoEVs promoted osteogenic differentiation. The *in vivo* study on the CIA mouse model further demonstrated that apoEVs could couple various functions and exert synergistic effects on the joint with RA, as evidenced by the regression of synovial inflammation, the reversal of cartilage damage and bone erosion, and the preservation of joint structure. These findings demonstrated that Mφ-apoEVs and OC-apoEVs contributed to restoring the homeostasis of the overall microenvironment in the RA joint and highlighted their potential application as a promising alternative to treat RA.

1. Introduction

Rheumatoid arthritis (RA) is an autoimmune disease characterized by synovial inflammation, cartilage destruction, and bone erosion, which affects up to 5–10 ‰ of the population worldwide [1]. Patients suffer from irreversible joint malformation and even disability in advanced RA. No radical cure for RA has been developed. Currently, the main treatment is to reduce pain and stop/slow further joint damage with disease-modifying antirheumatic drugs (DMARDs). In the RA joint, numerous inflammatory cells overproduce reactive oxidative species, proinflammatory mediators, and various proteases to create a highly inflammatory and tissue-damaging microenvironment. Meanwhile, the repair and regeneration of bone and cartilage are absent due to the lack of prorepairing stimuli [2,3]. Glucocorticoids, which exert good anti-inflammatory effects, are one of the most widely used DMARDs in the treatment of RA. However, the long-term use of glucocorticoids, such as dexamethasone (DEX), is hampered by many adverse effects, including an increased risk of infection, and osteoporosis [4,5]. In addition, glucocorticoids may suppress the regenerative capacity of bone and cartilage tissue [6]. Recent approaches for RA treatment using anti-inflammatory nanoparticles [7,8] have been reported. However, their application is also limited because they were unable to stimulate the repair process in the joints. Therefore, it is desirable to develop new strategies as alternatives to DMARDs that not only resolve inflammation

Peer review under responsibility of KeAi Communications Co., Ltd.
* Corresponding author. School of Biomedical Sciences and Engineering, South China University of Technology, Guangzhou International Campus, Guangzhou, 511442, China.
** Corresponding author. National Engineering Research Center for Tissue Restoration and Reconstruction and Innovation Center for Tissue Restoration and Reconstruction, Guangzhou, 510006, China.
E-mail addresses: msxlfu@scut.edu.cn (X. Fu), imwangyj@scut.edu.cn (Y. Wang).

https://doi.org/10.1016/j.bioactmat.2023.11.019
Received 2 August 2023; Received in revised form 24 November 2023; Accepted 24 November 2023

but also promote tissue regeneration.

Apoptosis, known as the most common form of programmed cell death, is an ordered and orchestrated process of cell death. It is well-known that cells undergoing apoptosis cause no inflammation. Traditionally, this is attributed to the quick clearance of apoptotic cells by phagocytes. Accumulating evidence shows that apoptotic cells regulate the immune response in a more active manner. Voll and colleagues first reported that the presence of apoptotic lymphocytes during monocyte activation increases their secretion of anti-inflammatory cytokines and decreases their secretion of proinflammatory cytokines [9]. Recently, studies have shown that the extracellular vesicles (EVs) generated by apoptotic cells (apoEVs), including apoptotic bodies, play an important role in regulating immune responses. For example, Zheng et al. reported that reduced M2 macrophages were recovered after efferocytosis of apoptotic vesicles derived from mesenchymal stem cells, whereas M1 macrophages were apparently decreased [10]. In addition to their immunosuppressive properties, apoptotic cells and apoEVs have been shown to be capable of stimulating cell proliferation and tissue regeneration [11,12]. Brock et al. found that apoptotic bodies could induce stem cell proliferation during epithelial tissue maintenance [13]. Xin et al. used apoptotic bodies derived from mesenchymal stem cells to treat intrauterine adhesions by inducing macrophage immunomodulation and tissue cell proliferation [14]. These studies highlight the potential of apoEVs in treating RA.

Similar to EVs derived from healthy cells, apoEVs inherit some special bioactive cargo from their parental cells. For instance, Qu et al. demonstrated that apoEVs derived from pluripotent stem cells accelerated wound healing via the retained SOX2 from their parental cells [15]. Both macrophages and osteoclasts are chief cells in the RA lesion. They actively participate in the modulation of the immune microenvironment and osteochondral homeostasis, respectively. Previous studies have shown that macrophage-derived EVs could induce macrophage polarization toward an M2 phenotype for the treatment of RA [16]. Small extracellular vesicles derived from osteoclasts promote bone formation through RANKL reverse signaling [17]. Therefore, we hypothesize that apoEVs derived from macrophages (Mφ-apoEVs) and osteoclasts (OC-apoEVs) may improve the immune microenvironment and stimulate the repair process of bone and cartilage simultaneously, thereby restoring homeostasis of the overall joint microenvironment.

In this study, Mφ-apoEVs and OC-apoEVs were harvested and purified from their parental cells. The regulatory effects of Mφ-apoEVs and OC-apoEVs on the phenotypes of key cells in the RA joint, including macrophages, chondrocytes, osteoclasts, and bone marrow mesenchymal stem cells (BMSCs), were systematically investigated *in vitro*. Next, the therapeutic effect of Mφ-apoEVs and OC-apoEVs on RA was evaluated in a collagen-induced arthritis (CIA) mouse model (see Scheme 1).

2. Materials and methods

2.1. Cell culture

Mouse bone marrow mesenchymal stem cells (BMSCs) and macrophages (RAW 264.7 cell line) were obtained from the Cell Bank of the Chinese Academy of Science. BMSCs were cultured with α-MEM (Gibco, USA), 10 % fetal bovine serum (FBS), and 1 % penicillin-streptomycin.

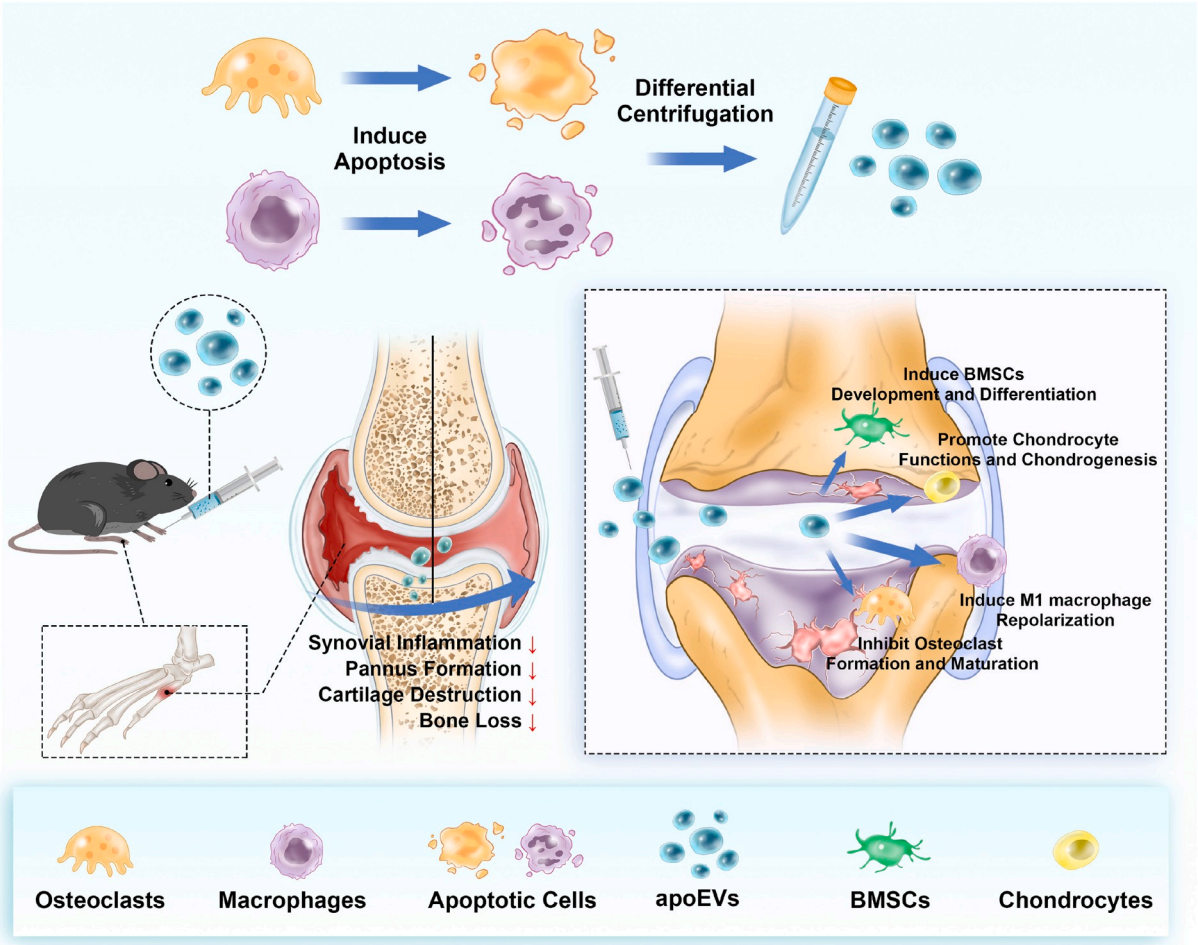

Scheme 1. Schematic illustration of Mφ-apoEVs/OC-apoEVs restoring homeostasis of the articular microenvironment for RA therapy.

Macrophages were cultured in DMEM (Gibco, USA) with 10 % FBS and 1 % penicillin-streptomycin. Macrophages were polarized to M1 by 100 ng/mL LPS (MedChemExpress, HY-D1056, USA) and 20 ng/mL IFN-γ (PeproTech, 315-05, USA) stimulation for 24 h [18], and were polarized to M2 by 40 ng/mL IL-4 (PeproTech, 214-14, USA) and 20 ng/mL IL-13 (PeproTech, 210-13, USA) stimulation for 48 h [19].

Osteoclasts were obtained by using the RAW 264.7 cell line, because RAW 264.7 cells can differentiate into osteoclast-like cells and have been used extensively in osteoclastogenesis studies [20,21]. To induce the osteoclastogenic differentiation of RAW 264.7 cells, the cells were seeded in 24-well plates at a density of 5×10^3 cells/cm^2, and treated with 50 ng/mL RANKL (R&D, 462-TEC/CF, USA) for 120 h. The medium was routinely changed every 60 h. The obtained osteoclasts were cultured in α-MEM (Gibco, USA), 10 % FBS, and 1 % penicillin-streptomycin.

Primary articular cartilage chondrocytes were isolated as previously described [22]. In brief, cartilage tissue was harvested and diced, and then the tissue was digested in 2 mg/mL type II collagenase (Gibco, 17101015, USA) at 37 °C overnight. The mixture was filtered through a 40 μm sieve, and then centrifuged for 10 min at 300 g. The collected chondrocytes were cultured in α-MEM (Gibco, USA), 10 % FBS, and 1 % penicillin-streptomycin.

All cells were cultured at 37 °C in a humidified 5 % CO_2 atmosphere.

2.2. Production and characterization of apoEVs

Cells were treated with 1 μM staurosporine (STS) (MedChemExpress, AM-2282, USA) for 6 h to induce cell apoptosis. The separation of apoEVs from apoptotic macrophages and osteoclast media was performed as previously described [14] with minor modifications. Briefly, the culture media was centrifuged at 300×*g* for 10 min to remove the remaining cells. Then, dead cells and cell debris were removed by centrifugation at 3000×*g* for 10 min. The supernatant was further centrifuged at 15,000×*g* for 60 min (Eppendorf, 5804R, Germany) to collect apoEVs. The apoEVs pellet was washed once with PBS and then centrifuged again. Finally, the apoEVs pellet was resuspended in PBS and stored at 4 °C.

For transmission electron microscopy (TEM) images of apoEVs, apoEVs samples were transferred to copper grids. Then, the samples were negatively stained with 2 % phosphotungstic acid. Images were taken with TEM (Thermo Fisher, Talos L120c, USA).

2.3. Histology staining for cells

To evaluate the function of osteoclasts, TRAP staining and F-actin staining were performed. For TRAP staining, cells were fixed in 4 % paraformaldehyde and then stained with the TRAP kit (Wako, 294-67001, Japan) according to the manufacturer's protocol. For staining of F-actin, cells were fixed with 4 % paraformaldehyde. Then, the cells were incubated with phalloidin (Abcam, ab176753, USA).

Glycosaminoglycan synthesis in ATDC5 cells was evaluated by staining with Alcian blue. Cells were fixed in 4 % paraformaldehyde and stained with 1 % Alcian blue 8GX (Cyagen, ALCB-10001, USA) in 0.1 M HCl overnight.

For alkaline phosphatase (ALP) staining of BMSCs, cells were fixed with 4 % paraformaldehyde and stained using ALP dye (Wako, 294-67001, Japan). To detect mineralized nodule formation by BMSCs, the cells were fixed with 4 % paraformaldehyde and stained with Alizarin red S (ARS) solution (Cyagen, ALIR-10001, USA).

For immunofluorescence staining, the cells were fixed with 4 % paraformaldehyde and permeabilized with Triton X-100. After blocking with 5 % BSA, the cells were incubated with the following primary antibodies: iNOS antibody (Affinity, AF0199, USA) and type II collagen antibody (Affinity, AF0135, USA). The cells were further incubated with goat Anti-Rabbit IgG (H + L) conjugated with Fluor 647 (Affinity, S0013, USA).

The bright field images were captured by optical microscopy (Leica, DMi1, Germany). The fluorescently stained samples were observed using confocal microscopy (Leica, TCS SP8, Germany).

2.4. Total collagen quantification and ALP activity assay

Sirius red (Chondrex, 9062, USA) was used to detect the total collagen content in ATDC5 cells according to the manufacturer's protocol. The optical density at 550 nm was measured using a microplate reader (TECAN, Infinite M 200 PRO NanoQuant, Switzerland).

For quantitative analysis of an ALP activity, cells were lysed with RIPA buffer and then tested with ALP assay kit (Beyotime, P0321, China) according to the manufacturer's protocol.

2.5. Cellular uptake

For the cellular uptake assay, cells were seeded onto a confocal dish and cultured with DiD (Thermo Fisher, V22887, USA)-labeled apoEVs (0.5 μg protein/10^5 cells). Then, the cells were fixed with 4 % paraformaldehyde, the nuclei were stained with DAPI (Beyotime, C1002, China) and the cytoskeleton was stained with phalloidin (Abcam, ab176753, USA). Fluorescence imaging was acquired via confocal microscopy (Leica, TCS SP8, Germany).

2.6. Flow cytometry analysis

The intensity of the forward scatter (FSC) signal is proportional to the particle size. Thus, the size of apoEVs was analyzed using the FSC signal by comparison with that of a population of microsphere standards (Thermo Fisher, F-13838, USA) with known diameters (1 μm, 2 μm, 4 μm, and 6 μm).

Annexin V apoptosis detection kits (Beyotime, C1077, China) were used to mark apoptotic cells and apoEVs. For cell biomarker analysis, cells were fixed with 4 % paraformaldehyde and permeabilized with saponin. Then, the fixed cells were incubated with antibodies in 5 % BSA. After washing with PBS, the stained cells were analyzed with flow cytometry (BD, LSRFortessa™, USA). The antibodies used in this study were CD206 antibody (Thermo Fisher, 17-2061-80, USA) and CCR7 antibody (Thermo Fisher, 12-1971-82, USA).

2.7. Enzyme linked immunosorbent assay (ELISA)

The culture supernatants were collected and cleared by centrifugation to remove dead cells and cell debris. The concentrations of TGF-β1 (R&D, DY1679, USA), TNF-α (Elabscience, E-EL-M0049c, China) and Arg1 (Elabscience, E-EL-M0154c, China) were measured using ELISA kits following the manufacturer's protocol.

2.8. qRT-PCR analysis

Total RNA was extracted from cells with TRIzol reagent and isolated with columns (BBI, B511321, China). A cDNA synthesis kit (GeneCopoeia, QP006, USA) was used to perform reverse transcription. qRT-PCR was performed in a QuantStudio™6Flex system (Thermo Fisher, USA) using SYBR® Green (GeneCopoeia, QP001, USA). The relative expression of target genes was normalized to that of GAPDH, and the $2^{-\Delta\Delta Ct}$ method was used to calculate the fold changes. The sequences of primers used in this study are listed in Table S1.

2.9. Proteomic analysis

Protein lysates of macrophages, apoptotic macrophages, Mφ-apoEVs, osteoclasts, apoptotic osteoclasts, and OC-apoEVs were prepared and subjected to LC-MS/MS analysis. The raw data were analyzed using Proteome Discoverer software. Proteins were identified by comparison against the UniProt database with the false discovery rate (FDR) set at 1

% for both peptides and proteins. Proteins that were significantly differentially expressed (fold change >1.5, P value < 0.05) were selected for further functional analysis based on Gene Ontology (GO) and Kyoto Encyclopedia of Genes and Genomes (KEGG) databases.

2.10. Induction of the collagen-induced arthritis (CIA) mouse model and treatment

All animal experiments were carefully performed in accordance with the International Guide for the Care and Use of the Laboratory Animals and approved by Laboratory Animal Research Center of South China University of Technology (2021051). Healthy DBA/1J mice (6–8 weeks old) were purchased from GemPharmatech Co. Ltd. and raised in specific pathogen-free (SPF) conditions. The CIA mouse model was prepared as previously described with some modifications [23]. Briefly, DBA/1J mice were injected intradermally at the base of the tail with 100 μg bovine type II collagen (Chondrex, 20022, USA) emulsified in 100 μL complete Freund's adjuvant (Chondrex, 7001, USA). Twenty-one days after the first immunization, the booster immunization was carried out with incomplete Freund's adjuvant (Chondrex, 7002, USA).

Limited by the narrow joint space, the footpad injection method was chosen for animal research. Twenty-eighy days after the first immunization, CIA mice were randomly assigned into three groups that received saline, DEX (0.1 mg/kg body weight), and apoEVs (5 μg protein/10 μL) by footpad injected into each footpad every 3 days. In each group, four paw footpads of a mouse received the same treatment. The CIA mice were clinically scored every 3 days, where 0 = no evidence of erythema and swelling; 1 = erythema and mild swelling limited to the tarsals or ankle joint; 2 = erythema and mild swelling extending from the ankle to the tarsals; 3 = erythema and moderate swelling extending from the ankle to metatarsal joint; and 4 = erythema and severe swelling encompassing the ankle, foot, and digits [23]. These arthritis scores were summed to give a maximum possible score of 16 per mouse.

2.11. Cartilage permeation evaluation

For *in vivo* evaluation, DiD (Thermo Fisher, V22887, USA) -labeled Mφ-apoEVs or OC-apoEVs were injected into footpads. The ankle joints were harvested after 24 h and 72 h, respectively. For ex vivo cartilage, ankle joints were collected from mice and cocultured with DiD-labeled Mφ-apoEVs or OC-apoEVs. Sections of ankle joints were stained and visualized by confocal microscopy (Leica, TCS SP8, Germany).

2.12. Histological analysis of tissue

The ankle joints were fixed in 4 % paraformaldehyde, decalcified, and embedded in paraffin. After being sliced, the sections were stained with hematoxylin and eosin (H&E), toluidine blue, safranin O/fast green, and TRAP. These sections were observed by the slide scanner system (3DHistech, P250FLASH, Hungary).

The Mankin score was used (structure 0-6 points, cellular abnormalities 0-3 points, matrix staining 0-4 points, and tidemark integrity 0-1 point) to evaluate the cartilage tissue.

2.13. Microcomputed tomography (micro-CT)

For micro-CT analysis, the hind paws and ankle joints were harvested and fixed in 4 % paraformaldehyde. The specimens were scanned at 70 kV and 100 μA with an isotropic resolution of 20 μm by micro-CT (ZKKS-MCT-Sharp, China). The dataset was reconstructed to obtain 3D images. Bone morphometric parameters, including bone volume vs. tissue volume (BV/TV), bone surface vs. bone volume (BS/BV) and trabecular bone thickness (Tb.Th), were calculated by ZKKS-MicroCT4.1 software (China).

2.14. In vivo safety evaluation

Blood samples were collected via the orbital venous plexus and centrifuged at 3000 rpm for 15 min at 4 °C to collect serum. Alanine aminotransferase (ALT), aspartate aminotransferase (AST), creatinine (CREA) and urea levels were tested by an automatic aralyzer (HITACHI, 3100, Japan). Spleens, livers, kidneys, hearts and lungs were analyzed by H&E staining.

2.15. Statistical analysis

Three independent experiments and at least one triplicate per group were performed to assure repeatability and statistical significance. The results are expressed as the mean ± standard deviation (SD). Independent unpaired two-tailed Student's t-test was used for the comparison between two groups. One-way analysis of variance (ANOVA) with Tukey's multiple comparison was used for comparisons among multiple groups. A value of $p < 0.05$ was considered statistically significant.

3. Results

3.1. Isolation and characterization of apoEVs

The obtained osteoclasts were identified by examining osteoclast-specific characteristics and functions, including the expression of tartrate resistant acid phosphatase (TRAP), multinucleation, and formation of actin-rings. As shown in Fig. 1a, the positive staining of TRAP, and the formation of typical acting-rings, together with the multiple nuclei observed in a single cell, showed that macrophages successfully differentiated into osteoclasts. The apoEVs are produced by apoptotic macrophages and osteoclasts. Cell apoptosis induced by STS was confirmed by fluorescence images. The apoptotic characteristics of the cells became distinct with time, and cells showed the expression of caspase-3 and the exposure of phosphatidylserine (PS) on the outer plasma membrane (Fig. 1b and S1). Consistently, the FCM results showed that more than 80 % of the cells were Annexin V positive after 6 h. The isolated Mφ-apoEVs and OC-apoEVs also possessed the characteristics of their parental cells and Annexin V positive apoEVs exceeded 80 % (Fig. 1d). The morphology and size of Mφ-apoEVs and OC-apoEVs were examined by TEM (Fig. 1c). Both Mφ-apoEVs and OC-apoEVs exhibited a spherical shape with different sizes. We further analyzed the sizes of Mφ-apoEVs and OC-apoEVs via FCM by using microspheres with standard sizes as controls (Fig. 1e). The results showed that the sizes of Mφ-apoEVs and OC-apoEVs were widely distributed below 6 μm, with approximately 50.8 % Mφ-apoEVs and 39.5 % OC-apoEVs having diameters between 2 and 4 μm. The membrane potential of Mφ-apoEVs and OC-apoEVs was negative due to their cell membrane origin (Fig. S2).

To identify the proteomic features of apoEVs, we performed LC-MS/MS analysis. The corresponding proteomic profiles of the normal cells, apoptotic cells, and apoEVs after hierarchical cluster analysis are shown as heatmaps (Fig. S3). We found that apoptotic biomarkers were significantly upregulated in Mφ-apoEVs and OC-apoEVs compared with healthy macrophages and osteoclasts, respectively. Osteoclast-specific functional proteins, such as Ctsk, MMP9, and Nfatc1, were differentially expressed in OC-apoEVs compared with Mφ-apoEVs (Fig. 1f). The differences between the groups may be caused by the processes of apoptosis, extracellular vesicle formation, and the different functions of their parental cells. Based on the GO database, these differentially expressed proteins (DEPs) were annotated to terms in 'biological process', 'cellular component' and 'molecular function' GO categories (Fig. S4). For the 'biological process' category, there was an obvious enrichment of DEPs linked to 'metabolic process', 'growth' and 'immune system process', which was similar to other cell types derived from apoEVs [10].

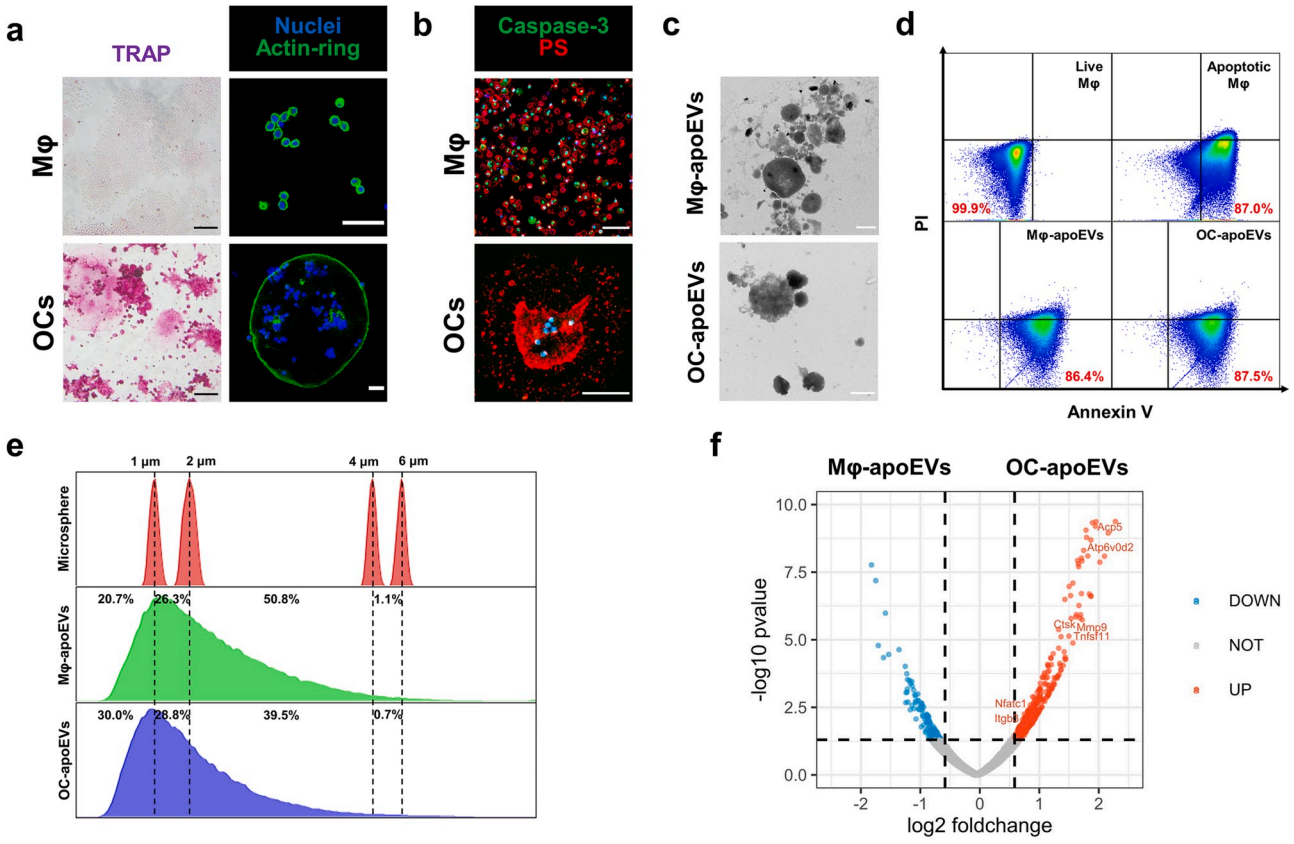

Fig. 1. Characterization of Mφ-apoEVs and OC-apoEVs. (a) Representative TRAP staining images and actin-ring staining images of macrophages and osteoclasts. (Scale bar, 50 μm) (b) Representative images of nuclei (blue), Caspase-3 (green), and PS (red) staining in apoptotic macrophages and osteoclasts. (Scale bar, 50 μm) (c) Representative TEM images showing the morphology of apoEVs. (Scale bar, 1 μm) (d) FCM analysis of Annexin V staining in cells and apoEVs. (e) FSC signal showing the size distribution of apoEVs. (f) Volcano plot showing significantly upregulated (red dots) and downregulated (blue dots) proteins in OC-apoEVs compared to Mφ-apoEVs. (Fold change >1.5, P value < 0.05).

3.2. *apoEVs induce the repolarization of M1 macrophages in vitro*

During the pathogenesis of RA, a large number of M1 macrophages infiltrate the synovium, overproducing proinflammatory mediators such as endogenous nitric oxide (NO), reactive oxygen species (ROS), and TNF-α, which promote inflammation, cartilage destruction, and bone erosion [24,25]. One effective therapeutic approach for RA is to switch the phenotype of macrophages from M1 to M2 [24–26]. Thus, we evaluated the effects of apoEVs on M1 macrophages. First, macrophages were incubated with fluorescently labeled Mφ-apoEVs and OC-apoEVs for 6 h to examine the cellular uptake of apoEVs. The IF images showed that a large number of Mφ-apoEVs and OC-apoEVs were internalized by macrophages (Fig. 2a). In this study, DEX, a synthetic small-molecule anti-inflammatory drug for RA treatment, was chosen as the control. To investigate the regulation of apoEVs on the repolarization of M1 macrophages, several representative markers of M1 and M2 macrophages were examined by FCM analysis (Fig. 2b). The expression of the M2 marker CD206 in M1 macrophages treated with DEX, Mφ-apoEVs, and OC-apoEVs was upregulated. Meanwhile, Mφ-apoEVs and OC-apoEVs significantly reduced the level of CCR7 in cells, which is usually expressed at a high level in M1 macrophages [27]. The inducible nitric oxide synthase (iNOS) of macrophages was also examined by IF (Fig. 2c and S5). Apparently, after treatment with Mφ-apoEVs and OC-apoEVs, the level of iNOS in M1 macrophages significantly decreased to a very low level, while that in cells treated with DEX remained high. NO production measured by the Griess assay exhibited a similar result (Fig. 2e). In addition, downregulated ROS levels were observed in the groups treated with DEX, Mφ-apoEVs, and OC-apoEVs (Fig. 2d). To further confirm that the phenotype of macrophages has been changed to anti-inflammatory, we monitored the production of representative pro- and anti-inflammatory cytokines secreted by macrophages with different treatments (Fig. 2f). Mφ-apoEVs and OC-apoEVs significantly inhibited the secretion of the proinflammatory cytokine TNF-α and stimulated the anti-inflammatory cytokines arginase-1 (Arg1) and TGF-β1. Although DEX treatment reduced the level of TNF-α in M1 macrophages, the secretion of Arg1 and TGF-β1 was still low. These results demonstrated that both Mφ-apoEVs and OC-apoEVs could induce M1 macrophages to repolarize toward the M2 phenotype.

3.3. *apoEVs promote chondrocyte functions and chondrogenesis in vitro*

Oxidative stress, proinflammatory mediators, and proteases block extracellular matrix (ECM) synthesis in chondrocytes [3,28]. Evidence suggests that inflammatory cytokines, such as interleukin 1β (IL-1β), inhibit type II collagen and glycosaminoglycan synthesis [25]. *In vitro*, IL-1β has been frequently used to simulate the inflammatory response of chondrocytes in arthritis. Thus, the effects of apoEVs on IL-1β stimulated chondrocytes were evaluated. To determine the uptake of chondrocytes, fluorescently labeled apoEVs were incubated with chondrocytes for 12 h, and endocytosis of Mφ-apoEVs and OC-apoEVs by chondrocytes was determined (Fig. 3a). The cellular uptake results showed that chondrocytes, although not professional phagocytes, internalized large amounts of Mφ-apoEVs and OC-apoEVs, suggesting that Mφ-apoEVs and OC-apoEVs can regulate chondrocytes through the intracellular delivery of bioactive contents. Stimulating chondrocytes for 7 d with IL-1β led to markedly reduced expression of type II collagen, the most abundant cartilage matrix protein. However, these effects of IL-1β on ECM metabolism were partly reversed in chondrocytes treated with DEX,

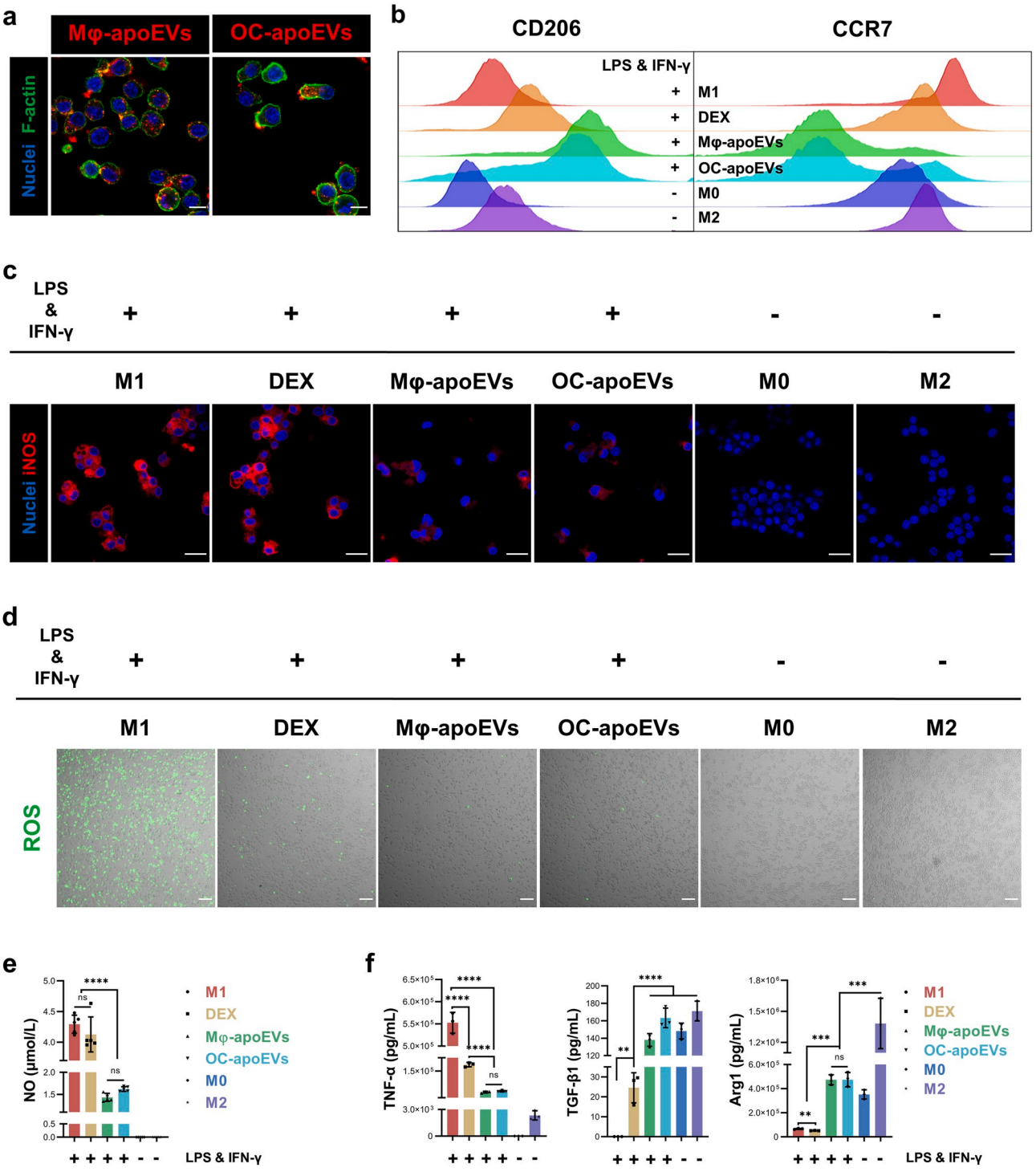

Fig. 2. Repolarization of macrophages from M1 toward M2 phenotype by apoEVs. (a) Representative images showing the cellular uptake of DiD-labeled apoEVs (red) by macrophages. (Scale bar, 20 μm) (b) FCM analysis of CD206 and CCR7 expression. (c) Representative images of iNOS (red) in macrophages. (Scale bar, 25 μm) (d) Representative images of ROS (green) production by macrophages. (Scale bar, 100 μm) (e) Concentration of NO in the culture medium by Griess assay. (n = 5) (f) Concentration of TNF-α, TGF-β1, and Arg1 in the culture medium by ELISA. (n = 3) (*p < 0.05, **p < 0.01, ***p < 0.001, ****p < 0.0001).

Mφ-apoEVs, and OC-apoEVs (Fig. 3b and S6).

Next, the effects of apoEVs on chondrogenesis were investigated using the chondrogenic cell line ATDC5. The results showed that DEX, Mφ-apoEVs, and OC-apoEVs induced increased expression of SOX9, a master transcription factor that drives chondrogenesis, compared to the control (Fig. 3c). Regarding cartilage matrix related genes, including COL2A1, PRG4, and COMP, DEX, Mφ-apoEVs, and OC-apoEVs also exhibited significant stimulatory effects. Cartilage matrix synthesis by ATDC5 cells was further assessed. The results of Alcian blue staining and Sirius red staining demonstrated higher levels of glycosaminoglycan deposition and total collagen content in the groups treated with DEX, Mφ-apoEVs, and OC-apoEVs than in the control group (Fig. 3d and S7).

According to the functional annotations based on the GO database, there was an obvious enrichment of DEPs related to 'extracellular matrix component' and 'collagen trimer' within the 'cellular component' category (Fig. S4). Further enrichment analysis revealed that Mφ-

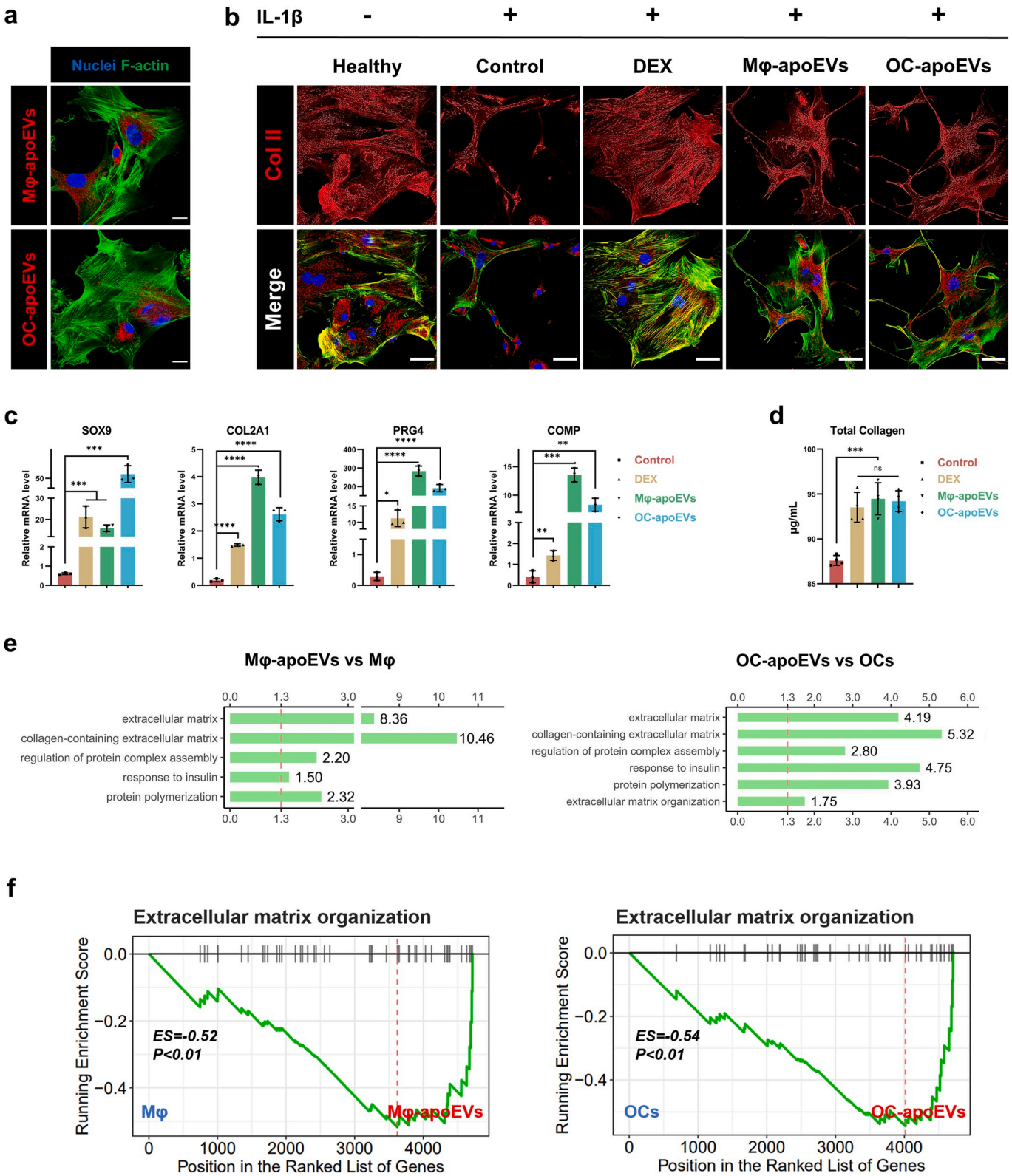

Fig. 3. Regulation of apoEVs on chondrocytes and ATDC5 cells. (a) Representative images showing the cellular uptake of DiD-labeled apoEVs (red) by chondrocytes. (Scale bar, 20 μm) (b) Representative images of type II collagen (red) in chondrocytes. (Scale bar, 50 μm) (c) Expression of chondrogenic genes measured by qRT-PCR. (n = 3) (d) Content of total collagen detected by Sirius red. (n = 4) (e) GO analysis showed that upregulated proteins in Mφ-apoEVs and OC-apoEVs were enriched in cartilage matrix associated terms. (f) KEGG pathway analysis showed that enriched proteins in Mφ-apoEVs and OC-apoEVs were more closely associated with extracellular matrix organization. (Fold change >1.5, P value < 0.05) (*p < 0.05, **p < 0.01, ***p < 0.001, ****p < 0.0001).

apoEVs and OC-apoEVs enclosed more proteins with ECM regulatory functions, including 'collagen-containing extracellular matrix' and 'regulation of protein complex assembly', respectively, than their parental cells (Fig. 3e). Moreover, we performed gene set enrichment analysis (GSEA), and the results suggested that these proteins were associated with 'extracellular matrix organization' (Fig. 3f). These findings indicated that Mφ-apoEVs and OC-apoEVs were enriched with a variety of functional proteins, which may contribute to their positive effects on chondrogenesis and cartilage matrix synthesis by chondrocytes.

3.4. apoEVs regulate osteoclastogenesis/osteogenesis in vitro

Osteoclast formation and activity are enhanced in RA joints. They play a key role in the pathogenesis of cartilage destruction and bone erosion [2]. To explore the effects of apoEVs on osteoclast differentiation, we treated RAW264.7 cells with DEX, Mφ-apoEVs, and OC-apoEVs in the presence of RANKL. RANKL stimulation significantly increased the expression of osteoclastic genes, including TRAP, MMP9, Cathepsin K, and Nfatc1, in cells, whereas DEX, Mφ-apoEVs, and OC-apoEVs treatment all suppressed these genes to varying degrees (Fig. 4a). Notably, when RAW264.7 cells were treated with Mφ-apoEVs and OC-apoEVs, the area of the actin-rings decreased greatly, whereas that in cells treated with DEX remained large, comparable to that in cells that

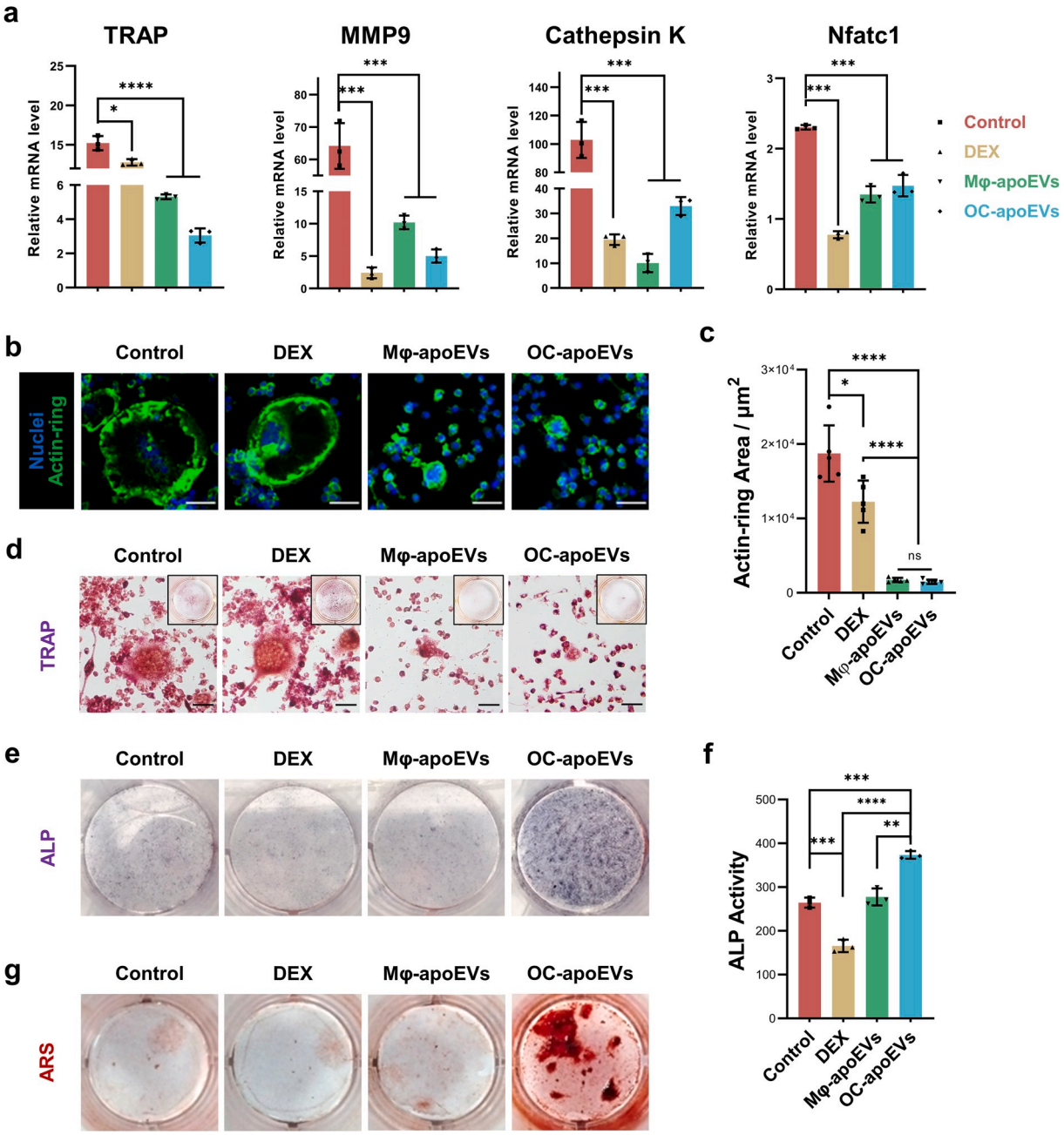

Fig. 4. Regulation of osteoclast and BMSC differentiation by apoEVs. (a) Expression of osteoclastogenic genes in cells measured by qRT-PCR. (n = 3) (b) Representative images of actin-ring staining (green) (scale bar, 50 μm) (c) Quantitative analysis of the actin-ring area. (n = 5) (d) Representative images of TRAP staining in cells. (Scale bar, 50 μm) (e) Representative images of ALP staining in cells. (f) Quantification analysis of ALP activity. (n = 3) (g) Representative images of ARS staining of mineralized nodules. (*p < 0.05, **p < 0.01, ***p < 0.001, ****p < 0.0001).

received no treatment (Fig. 4b-d). These results indicated that Mφ-apoEVs and OC-apoEVs effectively inhibited osteoclastogenesis in RAW264.7 cells. DEX also showed some inhibitory effects, although not as strong as apoEVs.

The effects of apoEVs on the osteogenesis of BMSCs were also evaluated. Surprisingly, only OC-apoEVs enhanced osteogenic differentiation, as evidenced by the increased ALP activity and the area of ARS-stained positive mineralized nodules (Fig. 4e-g). In contrast, an inappropriate concentration of DEX even showed a slight inhibitory effect on the osteogenic differentiation of BMSCs.

3.5. apoEVs relieve RA in the CIA mouse model

RA was successfully induced in DBA/1J mice, as evidenced by erythema, paw swelling, and weight loss (Figs. S8 and S9). The apoEVs were injected into the footpad every 3 days from day 28 to day 49 and saline and free DEX were used as the control groups (Fig. 5a). Chondrocytes are surrounded by a dense matrix of cartilage, which may prevent apoEVs from interacting with chondrocytes *in vivo*. The permeation of apoEVs in the cartilage matrix was determined. Apparently, a portion of Mφ-apoEVs and OC-apoEVs effectively permeated into cartilage and accumulated in the chondrocyte lacunae (Fig. 5b and S10).

We examined the pathological changes in the spleens, livers, kidneys, hearts, and lungs using H&E staining (Fig. S11). Compared to healthy mice, the spleens of CIA mice exhibited obvious red pulp congestion and an increase in lymphoid follicles in the white pulp. Local injections of free DEX, Mφ-apoEVs, and OC-apoEVs did not make any significant differences. Compared with healthy mice, the livers of CIA mice showed increased inflammatory cell infiltration, which was not alleviated in the free DEX, Mφ-apoEVs- and OC-apoEVs-treated groups. Next, the indicators of liver toxicity (AST and ALT) and kidney toxicity (CREA and UREA) were determined (Fig. S12). The values of all groups

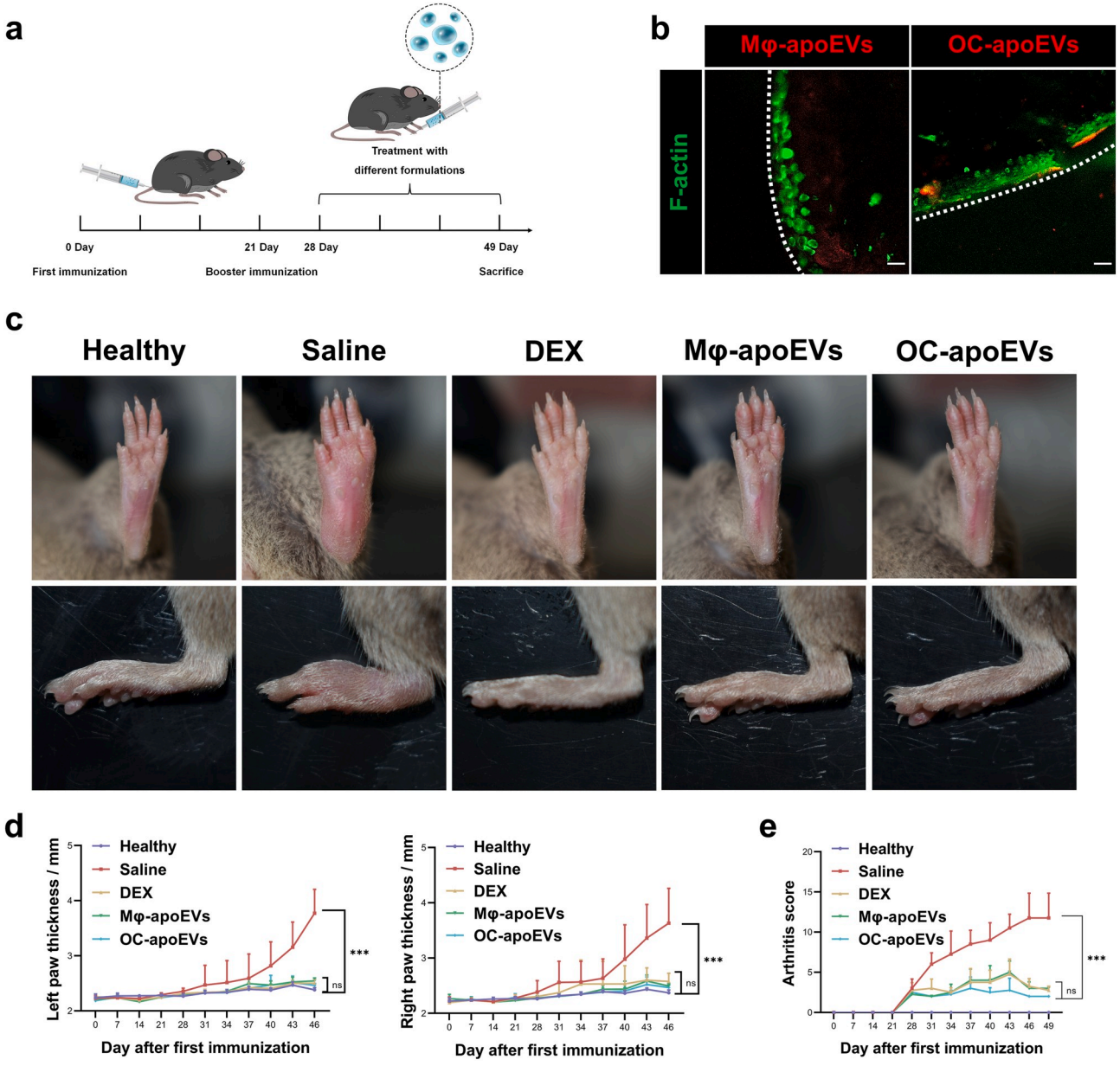

Fig. 5. Suppression of inflammation by apoEVs *in vivo*. (a) Schematic diagram of CIA mouse model establishment and treatment protocol. (b) Representative images showing the permeation of apoEVs into cartilage *in vivo*. (scale bar, 25 μm) (c) Representative images of hind paws of healthy mice and CIA mice treated with different formulations. (d) Paw thickness and (e) arthritis score of healthy mice and CIA mice treated with different formulations. (n = 7) (*p < 0.05, **p < 0.01, ***p < 0.001, ****p < 0.0001).

were within the normal range, and there was no significant difference among all groups. Apparently, no evidence showed that local injection of free DEX, Mφ-apoEVs, and OC-apoEVs caused any additional injuries to the chief organs of CIA mice. The weight loss and pathological changes in the spleen and liver are mainly due to the systemic chronic inflammation caused by RA. Although footpad injection of free DEX, Mφ-apoEVs and OC-apoEVs relieve the symptoms of arthritis, these treatments seem unable to alleciate the impact of systemic inflammation on organs, probably because of their limited diffusion via local injection.

The severity of joint swelling and paw thickness, together with the arthritis score were monitored during the whole experimental period, and used as a direct indicator of RA. As shown in Fig. 5, mice in the saline-treated group exhibited the most serious joint swelling and the thickest paw thickness and reached the highest arthritis score, indicating severe progression of RA. The injection of free DEX, Mφ-apoEVs, and OC-apoEVs greatly relievedjoint swelling and decreased paw thickness, and mice in these groups also had lower arthritis scores.

At the animal research endpoint, H&E staining was performed to observe the inflammation in the ankle joints of different groups (Fig. 6a). Compared to healthy mice, the ankle joints of CIA mice treated with saline exhibited severe inflammatory cell infiltration, synovial hyperplasia, and pannus formation. In contrast, the number of inflammatory cells was significantly reduced in the synovial zone in the free DEX, Mφ-apoEVs-, and OC-apoEVs-treated groups. In addition, no obvious synovial hyperplasia or pannus formation was observed in these three groups. To explore the reprogramming of pro-inflammatory M1 macrophages into anti-inflammatory M2 macrophages *in vivo*, we first assessed the expression of specific phenotypic markers of M1 (CD86) and M2 (CD206) macrophages in arthritic joint sections from CIA mice by immunohistochemical analysis (Fig. 6b). CD86 expression was markedly increased in the joint tissue of saline-treated CIA mice. While DEX, Mφ-apoEVs, and OC-apoEVs treatment simultaneously decreased CD86 expression and increased CD206 expressing, implying an efficient switch of joint-resident macrophages toward M2 phenotype.

With respect to the effects of apoEVs on the structure of cartilage tissue, as shown by H&E staining (Fig. 6a), significant morphological changes in articular cartilage and a significant decrease in the number of chondrocytes were observed in the saline-treated CIA mice compared with the healthy mice. In contrast, the cartilage surface was almost intact, and chondrocyte degeneration was much less obvious in the groups treated with free DEX, Mφ-apoEVs, and OC-apoEVs. To subsequently analyze the glycosaminoglycan content in articular cartilage, sections were stained with toluidine blue and Safranin O/fast green (Fig. 7a and b). Compared with the saline group, the apoEVs-treated groups exhibited an intensive increase in glycosaminoglycan content throughout the articular cartilage, almost the same as that in the healthy cartilage. DEX treatment also showed some positive effects on glycosaminoglycan content, but these effects were not as strong as those of apoEVs. To explore the regulation of apoEVs on extracellular matrix organization *in vivo*, we assessed type II collagen in arthritic joint

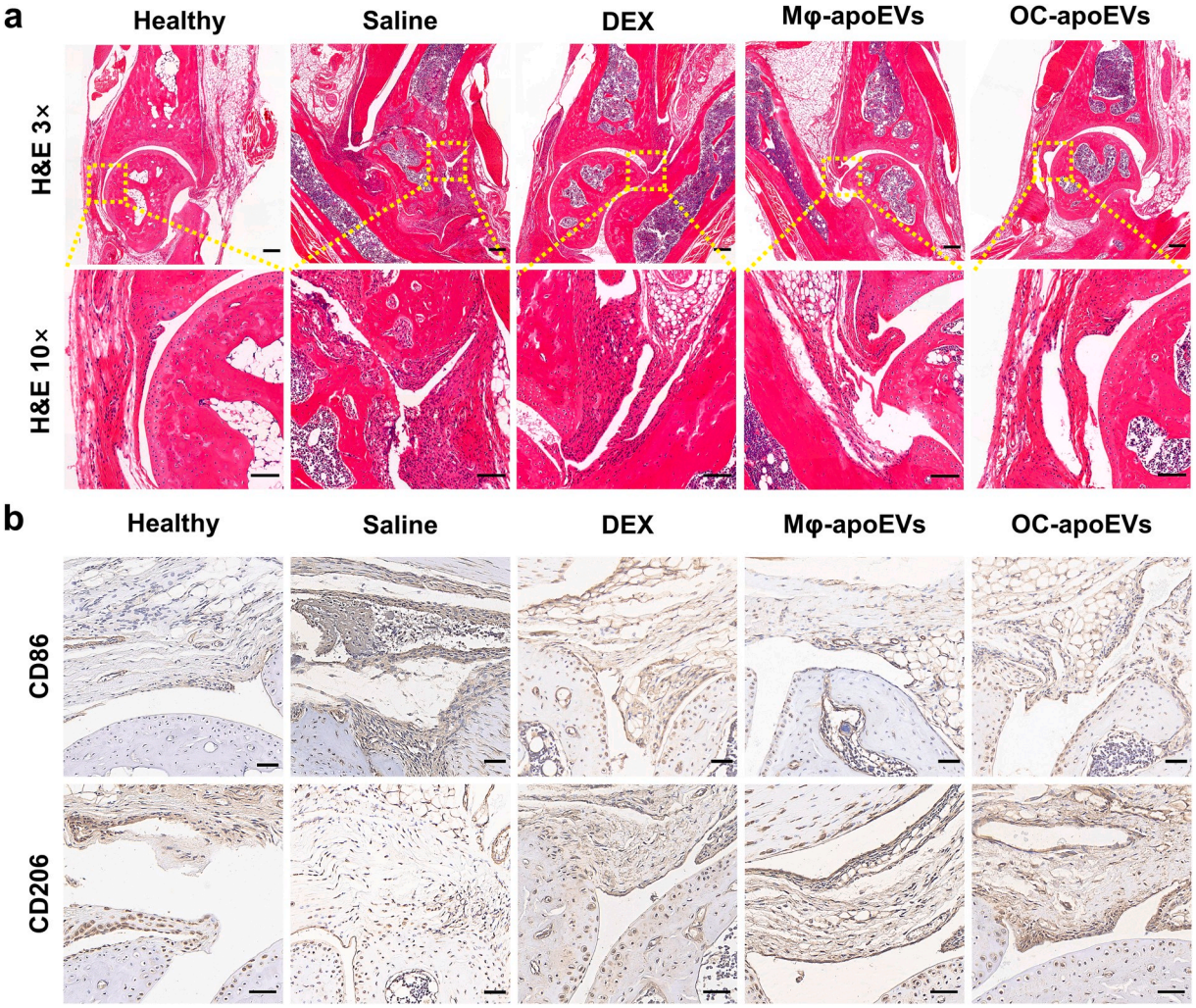

Fig. 6. Inflammation regulatory effects of apoEVs *in vivo*. (a) Representative H&E staining images. (H&E staining images: magnification 3×, Scale bar, 200 μm; magnification 10×, 100 μm) (b) Representative images of CD86 and CD206 immunohistochemical staining. (Scale bar, 50 μm).

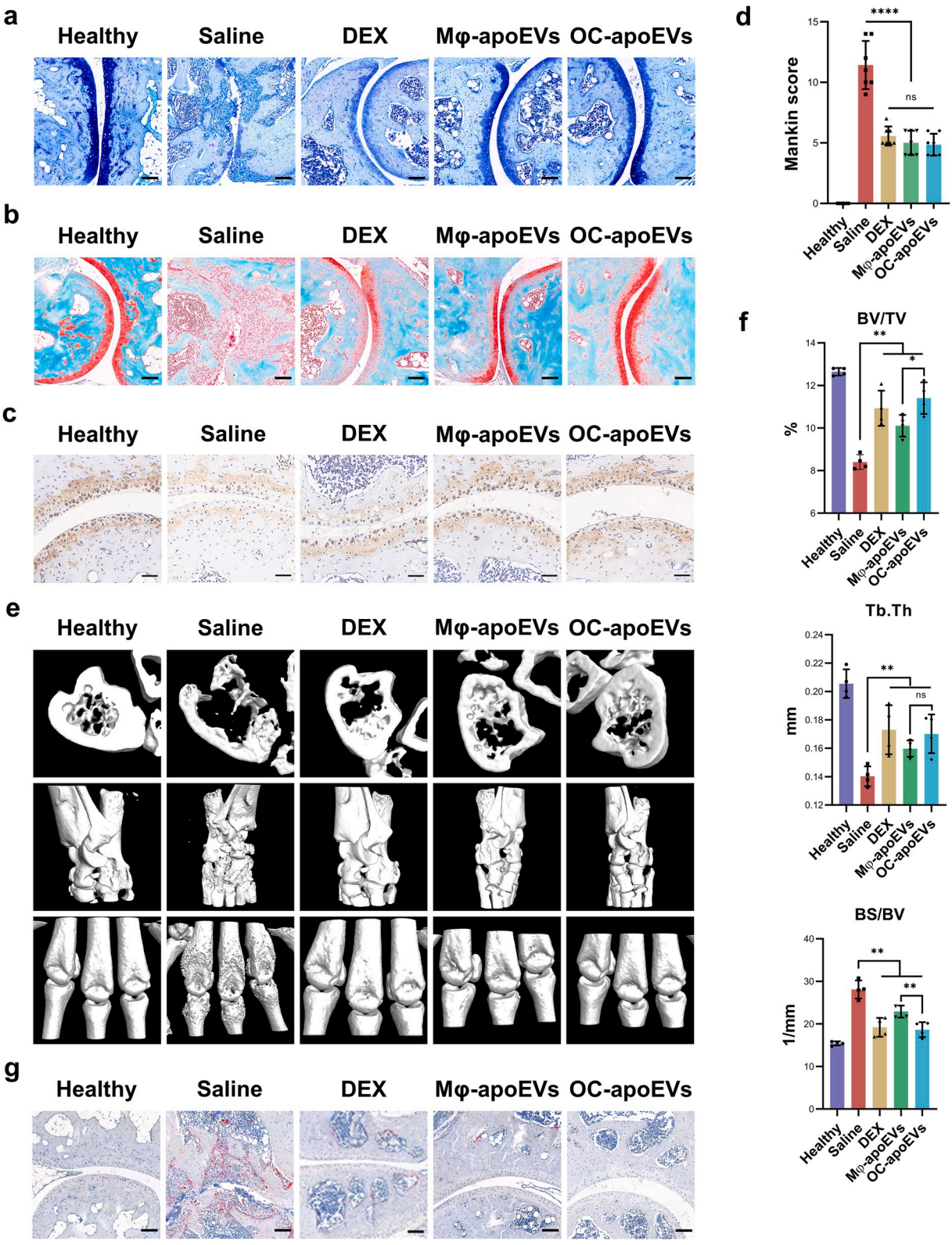

Fig. 7. Cartilage/bone regulatory effects of apoEVs *in vivo*. Representative (a) Toluidine blue staining images, and (b) Safranin O/fast green staining images of ankle joints from healthy mice and CIA mice treated with different formulations. (Scale bar, 100 μm) (c) Representative images of type II collagen immunohistochemical staining. (Scale bar, 50 μm). (d) Mankin score of healthy mice and CIA mice treated with different formulations. (n = 4) (e) Representative 3D-reconstructed images of hind paws by micro-CT analysis. (f) Quantitative analysis of BV/TV, BS/BV, and Tb.Th levels. (n = 4) (g) Representative TRAP staining images of ankle joints of healthy mice and CIA mice treated with different formulations. (Scale bar, 100 μm) (*p < 0.05, **p < 0.01, ***p < 0 0.001, ****p < 0.0001).

sections from CIA mice by immunohistochemical analysis (Fig. 7c). The synthesis of type II collagen was markedly decreased in the joint tissue of saline-treated CIA mice. While DEX, Mφ-apoEVs, and OC-apoEVs treatment increased type II collagen expression. Furthermore, the degradation level of articular cartilage was investigated by using the Mankin score, which assessed cartilage structure, cellularity, glycosaminoglycan depletion, and tidemark integrity (Fig. 7d). As expected, the average Mankin score was much higher in the saline-treated group (12.000 ± 1.871) than in the free DEX (2.400 ± 0.894), Mφ-apoEVs (2.200 ± 0.447), and OC-apoEVs (2.400 ± 0.894) treated groups.

To further evaluate the effects of apoEVs on bone, micro-CT imaging was used to assess the erosion of bone in the RA lesion (Fig. 7e). The 3D images showed that the ankles and toe joints in the saline-treated group exhibited a rough surface and suffered serious bone erosion compared with healthy mice. CIA mice treated with free DEX, Mφ-apoEVs, and OC-apoEVs displayed a smoother bone surface and less bone erosion than mice treated with saline. Moreover, morphometric parameters, including BV/TV, BS/BV, and Tb.Th, were calculated for quantitative analysis (Fig. 7f). The saline-treated group exhibited the lowest BV/TV and Tb.Th, and the highest BS/BV, while the values of the free DEX, Mφ-apoEVs-, and OC-apoEVs-treated groups were significantly improved. Consistent with the *in vitro* results, the highest BV/TV and Tb.Th together with the lowest BS/BV were observed in the mice treated with OC-apoEVs among all CIA mice, confirming its strongest effects in promoting bone formation. In addition, we performed TRAP staining to observe the abundance and distribution of osteoclasts in ankle joints (Fig. 7g). The results showed that osteoclasts were mainly located in the area of bone erosion, and the number of osteoclasts in the saline-treated group was the largest among all groups. In line with the *in vitro* results, injection of free DEX, Mφ-apoEVs, and OC-apoEVs all reduced the number of osteoclasts in the RA lesion, with apoEVs being more effective than free DEX.

4. Discussion

The apoEVs have emerged as promising intercellular signal mediators that regulate multiple physiological and pathological processes. The therapeutic effects of apoEVs derived from stem cells have been demonstrated in type 2 diabetes [10], intrauterine adhesions [14], skin wounds [15], osteopenia [12], and so forth. The articular microenvironment is a sophisticated system composed of a variety of extracellular matrix components, soluble factors, and cells. The microenvironment imbalance caused by the dysregulation of pro-/anti-inflammatory mediators and an imbalance in extracellular matrix remodeling greatly contribute to the pathogenic development of RA [1]. In this study, we have shown that apoEVs derived from macrophages and osteoclasts could significantly restore homeostasis of the articular microenvironment to alleviate the symptoms of RA through regulating key players in the joint, including macrophages, chondrocytes, BMSCs, and osteoclasts. Notably, OC-apoEVs exhibited a stronger capability in promoting osteogenic differentiation and the associated bone formation.

The apoEVs are a heterogeneous population of naturally occurring nano-to micro-sized membrane vesicles released by apoptotic cells. Compared with EVs derived from healthy cells, apoEVs lack the basic criteria for characterization and classification. PS is usually used as a simple indicator of apoptotic cells and apoEVs, although a subset of apoptotic bodies with low PS levels on the surface has been identified [29]. In our study, 86.4 % of Mφ-apoEVs and 87.5 % of OC-apoEVs were PS positive, suggesting that not all collected vesicles were apoEVs. There may be a very small portion of exosomes and other small extracellular vesicles present in the system because not all cells undergo apoptosis. The majority of EVs on RA can be mainly attributed to apoEVs. Size is one of the criteria for categorizing apoEVs. Smaller apoEVs with diameters ranging from 0.1 μm to 1 μm are referred to as apoptotic microvesicles, whereas larger apoEVs with diameters ranging from 1 μm to 5 μm are referred to as apoptotic bodies [30,31]. Current research on apoEVs in biomedical applications mostly focuses on apoptotic microvesicles [10,15]. However, apoptotic bodies have long been demonstrated to play an essential role in apoptosis induced immunosuppression [32,33]. Therefore, apoptotic bodies were not excluded from the apoEVs. As shown in Fig. 1c and e, the collected apoEVs were a group of particles with sizes widely distributed between 0.1 and 5 μm. Although it may be relatively difficult for large apoptotic bodies to penetrate into dense cartilage and bone (Fig. 5b), they can modulate the synovial microenvironment, thereby helping resolve joint inflammation. It has been reported that healthy osteoblast-derived microvesicles with diameters of approximately 400 nm suppress osteoblast differentiation and promote osteoclastogenesis, while the subset with sizes of approximately 200 nm cannot [34]. Thus, it is beneficial to further clarify the differences in functions between smaller and larger apoEVs.

The exact mechanisms by which apoptotic cells and EVs mediate inflammation, cell proliferation, and tissue regeneration are not fully understood. A number of factors contribute to their diverse functions. First and foremost, when cells undergo apoptosis, they acquire new cell surface determinants to send ‘eat me’ signals to responder phagocytes and suppress immune responses. Since these determinants (e.g., PS and calreticulin) are well conserved throughout metazoan evolution and their recognition shows neither species-specific nor tissue-specific restriction, it is believed that all apoptotic cells, regardless of their origins, have similar immune modulating capabilities [35]. Indeed, both Mφ-apoEVs and OC-apoEVs effectively inhibited the inflammatory functions of macrophages (Fig. 2). The phenotypic change of macrophages further leads to the improvement of the microenvironment, thereby affecting the function of other types of tissue cells (e.g., chondrocytes, MSCs, and osteoclasts) in the joint [36]. For example, TNF-α secreted by M1 macrophages promotes osteoclastogenesis, whereas IL-10 secreted by M2 macrophages inhibits osteoclastogenesis [37]. Thus, the observed reduced osteoclast formation and maturation may be at least partially attributed to the apoEVs-induced M2 repolarization of macrophages. Meanwhile, our results (Fig. 4) together with some other reports have demonstrated that apoEVs directly affect MSCs [12,13]. Thus, Mφ-apoEVs and OC-apoEVs may also be taken up by local MSCs and enhance the proliferation and chondrogenic/osteogenic differentiation of MSCs. In addition to cell surface determinants, recent studies have shown that the apoptotic metabolite secretum induces specific gene programs in neighboring cells [38,39], indicating that the cargo within apoptotic cells and EVs is also important. This may explain the different effects of Mφ-apoEVs and OC-apoEVs on osteogenesis and bone formation. OC-apoEVs were able to induce osteogenic differentiation *in vitro* and bone formation *in vivo* more efficiently than Mφ-apoEVs (Fig. 4e–g and Fig. 7e–g). Similarly, osteoclast-derived small extracellular vesicles [17] and apoptotic bodies [40] have been reported to enhance osteogenesis, indicating that some bioactive factors specifically from osteoclasts do this job. As expected, proteomic analysis demonstrated DEPs between macrophages and osteoclasts, which were inherited in apoptotic cells and apoEVs (Fig. S3). The importance of the cargo also highlights the potential of tailoring the function of apoEVs to meet the needs of distinct pathological microenvironments by selecting the parental cell types.

5. Conclusions

In summary, the present study demonstrated that Mφ-apoEVs and OC-apoEVs could trigger the M2 repolarization of macrophages, stimulate chondrocyte functions and chondrogenesis, and inhibit the formation and maturation of osteoclasts. In addition, OC-apoEVs in particular exhibited a significant enhancement in BMSC differentiation. The regulation of apoEVs on multiple tissue cells in the joints restored the homeostasis of the microenvironment in the RA joint, thereby protecting the integrity of the joint structure from malformation. These results highlight the potential of apoEVs, especially OC-apoEVs in RA

treatment.

Ethics approval and consent to participate

All animal experiments were carefully performed in accordance with the International Guide for the Care and Use of Laboratory Animals and approved by the Laboratory Animal Research Center of South China University of Technology (#2021051).

CRediT authorship contribution statement

Xian Li: Writing – original draft, Investigation, Formal analysis, Data curation. **Shichun Li:** Investigation, Formal analysis. **Xiaoling Fu:** Writing – review & editing, Project administration, Funding acquisition, Conceptualization. **Yingjun Wang:** Project administration, Funding acquisition, Conceptualization.

Declaration of competing interest

The authors declare that they have no known competing financial interests or personal relationships that could have appeared to influence the work reported in this paper.

Acknowledgments

This work was supported by the National Natural Science Foundation of China (T2288101, 31971266, 82272152, U1801252), Guangdong Basic and Applied Basic Research Foundation (2022A1515011925), Science and Technology Program of Guangzhou (202206040001), and the Key Research and Development Program of Guangzhou (202007020002).

Appendix A. Supplementary data

Supplementary data to this article can be found online at https://doi.org/10.1016/j.bioactmat.2023.11.019.

References

[1] J.S. Smolen, D. Aletaha, I.B. McInnes, Rheumatoid arthritis, Lancet 388 (10055) (2016) 2023–2038.
[2] G. Schett, E. Gravallese, Bone erosion in rheumatoid arthritis: mechanisms, diagnosis and treatment, Nat. Rev. Rheumatol. 8 (2012) 656–664.
[3] H. Yang, Z. Yu, S. Ji, J. Yan, Y. kong, Q. Huo, Z. Zhang, Y. Niu, Y. Liu, Regulation of synovial macrophages polarization by mimicking efferocytosis for therapy of osteoarthritis, Adv. Funct. Mater. 32 (2022) 2207637.
[4] P. Chotiyarnwong, E.V. McCloskey, Pathogenesis of glucocorticoid-induced osteoporosis and options for treatment, Nat. Rev. Endocrinol. 16 (2020) 437–447.
[5] E. Wiebe, D. Huscher, D. Schaumburg, A. Palmowski, S. Hermann, T. Buttgereit, R. Biesen, G.R. Burmester, Y. Palmowski, M. Boers, J.H. Stone, C. Dejaco, F. Buttgereit, Optimising both disease control and glucocorticoid dosing is essential for bone protection in patients with rheumatic disease, Ann. Rheum. Dis. 81 (2022) 1313–1322.
[6] L. Chen, Z. Ni, J. Huang, R. Zhang, J. Zhang, B. Zhang, L. Kuang, X. Sun, D. Zhang, N. Su, H. Qi, J. Yang, M. Jin, F. Luo, H. Chen, S. Zhou, X. Du, J. Ouyang, Z. Wang, Y. Xie, Q. Tan, L. Chen, Long term usage of dexamethasone accelerating accelerates the initiation of osteoarthritis via enhancing chondrocyte apoptosis and the extracellular matrix calcification and apoptosis of chondrocytes, Int. J. Biol. Sci. 17 (2021) 4140–4153.
[7] H. Fang, Y. Sha, L. Yang, J. Jiang, L. Yin, J. Li, B. Li, B. Klumperman, Z. Zhong, F. Meng, Macrophage-targeted hydroxychloroquine nanotherapeutics for rheumatoid arthritis therapy, ACS Appl. Mater. Interfaces 14 (7) (2022) 8824–8837.
[8] L. Yang, Y. Sha, Y. Wei, H. Fang, J. Jiang, L. Yin, Z. Zhong, F. Meng, Mannose-mediated nanodelivery of methotrexate to macrophages augments rheumatoid arthritis therapy, Biomater. Sci. 11 (6) (2023) 2211–2220.
[9] R.E. Voll, M. Herrmann, E.A. Roth, C. Stach, J.R. Kalden, I. Girkontaite, Immunosuppressive effects of apoptotic cells, Nature 390 (1997) 350–351.
[10] C. Zheng, B. Sui, X. Zhang, J. Hu, J. Chen, J. Liu, D. Wu, Q. Ye, L. Xiang, X. Qiu, S. Liu, Z. Deng, J. Zhou, S. Liu, S. Shi, Y. Jin, Apoptotic vesicles restore liver macrophage homeostasis to counteract type 2 diabetes, J. Extracell. Vesicles 10 (2021) e12109.
[11] Y. Fuchs, H. Steller, Programmed cell death in animal development and disease, Cell 147 (2011) 742–758.
[12] D. Liu, X. Kou, C. Chen, S. Liu, Y. Liu, W. Yu, T. Yu, R. Yang, R. Wang, Y. Zhou, S. Shi, Circulating apoptotic bodies maintain mesenchymal stem cell homeostasis and ameliorate osteopenia via transferring multiple cellular factors, Cell Res. 28 (2018) 918–933.
[13] C.K. Brock, S.T. Wallin, O.E. Ruiz, K.M. Samms, A. Mandal, E.A. Sumner, G. T. Eisenhoffer, Stem cell proliferation is induced by apoptotic bodies from dying cells during epithelial tissue maintenance, Nat. Commun. 10 (2019) 1044.
[14] L. Xin, C. Wei, X. Tong, Y. Dai, D. Huang, J. Chen, L. Ma, S. Zhang, In situ delivery of apoptotic bodies derived from mesenchymal stem cells via a hyaluronic acid hydrogel: a therapy for intrauterine adhesions, Bioact. Mater. 12 (2022) 107–119.
[15] Y. Qu, Y. He, B. Meng, X. Zhang, J. Ding, X. Kou, W. Teng, S. Shi, Apoptotic vesicles inherit SOX2 from pluripotent stem cells to accelerate wound healing by energizing mesenchymal stem cells, Acta Biomater. 149 (2022) 258–272.
[16] H. Kim, J.H. Back, G. Han, S.J. Lee, Y.E. Park, M.B. Gu, Y. Yang, J.E. Lee, S.H. Kim, Extracellular vesicle-guided in situ reprogramming of synovial macrophages for the treatment of rheumatoid arthritis, Biomaterials 286 (2022) 121578.
[17] Y. Ikebuchi, S. Aoki, M. Honma, M. Hayashi, Y. Sugamori, M. Khan, Y. Kariya, G. Kato, Y. Tabata, J.M. Penninger, N. Udagawa, K. Aoki, H. Suzuki, Coupling of bone resorption and formation by RANKL reverse signalling, Nature 561 (2018) 195–200.
[18] Q. Wu, X. Fu, X. Li, J. Li, W. Han, Y. Wang, Modification of adipose mesenchymal stem cells-derived small extracellular vesicles with fibrin-targeting peptide CREKA for enhanced bone repair, Bioact. Mater. 20 (2023) 208–220.
[19] F.O. Martinez, L. Helming, S. Gordon, Alternative activation of macrophages: an immunologic functional perspective, Annu. Rev. Immunol. 27 (2009) 451–483.
[20] P. Collin-Osdoby, X. Yu, H. Zheng, P. Osdoby, RANKL-mediated osteoclast formation from murine RAW 264.7 cells, Methods Mol. Med. 80 (2012) 187–202.
[21] M. Li, X. Fu, H. Gao, Y. Ji, J. Li, Y. Wang, Regulation of an osteon-like concentric microgrooved surface on osteogenesis and osteoclastogenesis, Biomaterials 216 (2019) 119269.
[22] M. Gosset, F. Berenbaum, S. Thirion, C. Jacques, Primary culture and phenotyping of murine chondrocytes, Nat. Protoc. 3 (2008) 1253–1260.
[23] D.D. Brand, K.A. Latham, E.F. Rosloniec, Collagen-induced arthritis, Nat. Protoc. 2 (2007) 1269–1275.
[24] I.A. Udalova, A. Mantovani, M. Feldmann, Macrophage heterogeneity in the context of rheumatoid arthritis, Nat. Rev. Rheumatol. 12 (2016) 472–485.
[25] T.L. Fernandes, A.H. Gomoll, C. Lattermann, A.J. Hernandez, D.F. Bueno, M. T. Amano, Macrophage: a potential target on cartilage regeneration, Front. Immunol. 11 (2020) 111.
[26] G. Schett, M.F. Neurath, Resolution of chronic inflammatory disease: universal and tissue-specific concepts, Nat. Commun. 9 (2018) 3261.
[27] K. Van Raemdonck, S. Umar, K. Palasiewicz, S. Volkov, M.V. Volin, S. Arami, H. J. Chang, B. Zanotti, N. Sweiss, S. Shahrara, CCL21/CCR7 signaling in macrophages promotes joint inflammation and Th17-mediated osteoclast formation in rheumatoid arthritis, Cell. Mol. Life Sci. 77 (2020) 1387–1399.
[28] I.B. McInnes, G. Schett, Cytokines in the pathogenesis of rheumatoid arthritis, Nat. Rev. Immunol. 7 (2007) 429–442.
[29] I.K.H. Poon, M.A.F. Parkes, L. Jiang, G.K. Atkin-Smith, R. Tixeira, C.D. Gregory, D. C. Ozkocak, S.F. Rutter, S. Caruso, J.P. Santavanond, S. Paone, B. Shi, A.L. Hodge, M.D. Hulett, J.D.Y. Chow, T.K. Phan, A.A. Baxter, Moving beyond size and phosphatidylserine exposure: evidence for a diversity of apoptotic cell-derived extracellular vesicles in vitro, J. Extracell. Vesicles 8 (2019) 1608786.
[30] D. Karpman, A.L. Stahl, I. Arvidsson, Extracellular vesicles in renal disease, Nat. Rev. Nephrol. 13 (2017) 545–562.
[31] C. Lynch, M. Panagopoulou, C.D. Gregory, Extracellular vesicles arising from apoptotic cells in tumors: roles in cancer pathogenesis and potential clinical applications, Front. Immunol. 8 (2017) 1174.
[32] T.K. Phan, D.C. Ozkocak, I.K.H. Poon, Unleashing the therapeutic potential of apoptotic bodies, Biochem. Soc. Trans. 48 (2020) 2079–2088.
[33] X. Li, Y. Liu, X. Liu, J. Du, U.K. Bhawal, J. Xu, L. Guo, Y. Liu, Advances in the therapeutic effects of apoptotic bodies on systemic diseases, Int. J. Mol. Sci. 23 (2022) 8202.
[34] M. Uenaka, E. Yamashita, J. Kikuta, A. Morimoto, T. Ao, H. Mizuno, M. Furuya, T. Hasegawa, H. Tsukazaki, T. Sudo, K. Nishikawa, D. Okuzaki, D. Motooka, N. Kosaka, F. Sugihara, T. Boettger, T. Braun, T. Ochiya, M. Ishii, Osteoblast-derived vesicles induce a switch from bone-formation to bone-resorption in vivo, Nat. Commun. 13 (2022) 1066.
[35] R.B. Birge, S. Boeltz, S. Kumar, J. Carlson, J. Wanderley, D. Calianese, M. Barcinski, R.A. Brekken, X. Huang, J.T. Hutchins, B. Freimark, C. Empig, J. Mercer, A. J. Schroit, G. Schett, M. Herrmann, Phosphatidylserine is a global immunosuppressive signal in efferocytosis, infectious disease, and cancer, Cell Death Differ. 23 (2016) 962–978.
[36] Y. Sun, J. Li, X. Xie, F. Gu, Z. Sui, K. Zhang, T. Yu, Macrophage-osteoclast associations: origin, polarization, and subgroups, Front. Immunol. 12 (2021) 778078.
[37] H. Takayanagi, Osteoimmunology: shared mechanisms and crosstalk between the immune and bone systems, Nat. Rev. Immunol. 7 (2007) 292–304.
[38] M.L. Alegre, The anti-inflammatory function of the apoptotic secretome, Am. J. Transplant. 20 (6) (2020) 1471.
[39] A.A. Baxter, I.K. Poon, Apoptotic cells secrete metabolites to regulate immune homeostasis, Immunol. Cell Biol. 98 (2020) 355–357.
[40] Q. Ma, M. Liang, Y. Wu, N. Ding, L. Duan, T. Yu, Y. Bai, F. Kang, S. Dong, J. Xu, C. Dou, Mature osteoclast-derived apoptotic bodies promote osteogenic differentiation via RANKL-mediated reverse signaling, J. Biol. Chem. 294 (29) (2019) 11240–11247.